

# The impact of local resonance on the enhanced transmission and dispersion of surface resonances

Zeyong Wei, Jinxin Fu, Yang Cao, Chao Wu, and Hongqiang Li\*  
*Physics Department, Tongji University, 200092, Shanghai, China*

We investigate the enhanced microwave transmission through the array of metallic coaxial annular apertures (MCAAs) experimentally and theoretically. The even-mode and the odd-mode surface resonances are clarified from the spatial field distributions and the dispersion diagram. The impact of local resonance is thoroughly embodied in the even-mode surface resonant states, while the odd-mode surface resonances are scaled by periodicity, invariant to different local geometry of the unit cell, and invisible in measurements. The enhanced transmission is the collective selections on the interplay between the local resonances and the evanescent Bloch wave channels on the surface. Transmission measurements for different inner diameter of the apertures show that the transmissivity extrema with respect to the specific angles precisely correspond to the degenerate points in the dispersion diagram of surface resonances.

## I. INTRODUCTION

Extraordinary optical transmission (EOT) through a periodical array of subwavelength nano-holes in metal films[1] provides a new way to manipulate the light waves in subwavelength division. The origin of EOT was attributed to the resonant tunneling of surface plasmon polaritons (SPPs)[2]. Later studies found that the enhanced transmission can also be achieved in Terahertz[3] or microwave region[4] where the metal surface does not support SPPs but surface resonances[5]. The high transmission peak through more complicated apertures, such as coaxial apertures[6, 7], rectangular holes[8, 9], etc., tends to be red-shifted or even scaled by waveguide resonance instead of the periodicity[10]. Polarization-dependent transmission spectra as well as the optical activities are observed when the array of large-sized elliptical holes is adopted[11]. These studies strongly indicate that the local resonance is crucial and dominant to the formation of EOT under specific circumstances.

In this paper, we adopt the modal expansion method (MEM) to calculate the enhanced microwave transmission through the array of metallic coaxial annular apertures (MCAAs) as well as the dispersion of surface resonances. In microwave region, metals are perfect electric conductors (PECs), which enable us to easily characterize the spatial dispersion from the periodic structure. The even-mode and the odd-mode surface resonances are clarified by calculations on the transmission spectra, the spatial field distributions, and the dispersion diagram. The impact of local resonance is thoroughly embodied in the even-mode surface resonant states, while the odd-mode surface resonances are scaled by periodicity, invariant to different local geometry of the unit cell, and invisible in measurements. And the enhanced transmission comes from collective selections on the interplay between the local resonances and the evanescent Bloch wave channels on the surface. Transmissivity extrema with respect to the specific incident angles precisely correspond to the degenerate points in the dispersion diagram of surface resonances. The results are heuristic to the enhanced transmission in the optical region as well.

## II. SAMPLE DESCRIPTION AND EXPERIMENTAL SETUP

Our samples were fabricated on  $1\text{m}\times 1\text{m}$  copper slabs with a thickness of  $t = 2\text{mm}$ . As a first step to fabricate our samples, two-dimensional square arrays of air holes with a lattice constant  $p = 30\text{mm}$  were drilled through four identical copper plates, each hole has the same diameter  $D = 10\text{mm}$ ; Secondly, each air hole was embedded coaxially with an annular ring made of teflon with a dielectric constant  $\epsilon_r = 2.2$ . and an appropriate diameter  $d$ ; Finally, a copper cylinder with a diameter of  $d$  is embedded in the dielectric ring at the hole center. as shown in the inset of Fig.1. Four samples were fabricated with different inner diameters  $d = 8.3, 6.3, 5.0, 2.0\text{mm}$  respectively.

The transmission measurements are performed with Aglient network analyzer 8722ES in a microwave chamber. Three pairs of highly directive horn antennas with a gain factor of 24.8dB are utilized to cover the frequency range within  $5.8\sim 8.2$ ,  $8.2\sim 12.4$ , and  $12.4\sim 18.2\text{GHz}$  respectively. The sample plate is vertically positioned on a rotary table,

---

\*Electronic address: hqlee@tongji.edu.cn

at the center of the line between the emitting and the receiving horns, the horn antennas are 5.0 meters apart from each other. Oblique incidence is achieved by rotating the sample plate axially about  $y$  axis. Horizontal( $\vec{E}||\hat{x}$ ) or vertical polarized ( $\vec{E}||\hat{y}$ ) Gaussian beams from the horns give rise to the  $TM$  or  $TE$  polarized incidence. Transmissivity through the sample plate is normalized to the wave energy transmitted between the two horn antennas in free space without the sample plate.

### III. MODAL EXPANSION THEORY

The modal expansion method[12] is a powerful tool to calculate the transmission of layered system, for example, one-dimensional metallic grating. The essence of the method is that the electromagnetic wave fields in the specific layers can be decomposed with a series of in-plane eigen-functions correspondingly. The problem can be solved by applying boundary continuum condition at all interfaces. At low frequency region, the wave fields inside the aperture mainly determined by the fundamental waveguide mode, so that the method can be simplified to one-mode theory[13] which is fast and convergent.

With the notions stated above, we develop the modal expansion method to deal with two-dimensional(2D) array of MCAAs. We note that the plane wave incidence can not excite  $TEM$  guided mode and all the  $TM$  guided modes in a coaxial aperture accounting for its in-plane symmetry. So we only consider the  $TE_{p,q}$  guided mode inside the MCAAs, where the integer pair  $(p, q)$  denotes the mode number[14]. The magnetic field inside the MCAAs within the region of  $0 < z < h$  can be written as the superposition of all the forward and backward  $TE_{p,q}$  modes:

$$\vec{H}^{II} = \sum_{p=1}^{\infty} \sum_{q=1}^{\infty} (a_{p,q} e^{-i\beta_{p,q}z} - b_{p,q} e^{i\beta_{p,q}z}) \beta_{p,q} \vec{g}_{p,q}(x, y), \quad (1)$$

where  $a_{p,q}$  and  $b_{p,q}$  are the coefficients of the  $(p, q)^{th}$  order of forward and backward guided waves,  $\beta_{p,q}$  is the wavevector along  $z$  axis with  $\beta_{p,q} = \sqrt{k^2 - T_{p,q}^2}$ , and  $T_{p,q}$  is the  $q^{th}$  root of eigen function  $J'_p(Td/2)N'_p(TD/2) - J'_p(TD/2)N'_p(Td/2) = 0$ .  $\vec{g}_{p,q}(x, y)$  is the in-plane mode profile of the  $(p, q)^{th}$  order of guided wave, which can be expressed with  $\vec{g}_{p,q}(x, y) = g_{\rho,p,q}(\rho, \phi)\hat{e}_\rho + g_{\phi,p,q}(\rho, \phi)\hat{e}_\phi$  in cylinder coordinates, where

$$\begin{aligned} g_{\rho,p,q}(\rho, \phi) &= [N'_p(T_{p,q}d/2)J'_p(T_{p,q}\rho) - J'_p(T_{p,q}d/2)N'_p(T_{p,q}\rho)] \sin(p\phi) \\ g_{\phi,p,q}(\rho, \phi) &= -\frac{\rho}{\rho} [N'_p(T_{p,q}d/2)J_p(T_{p,q}\rho) - J'_p(T_{p,q}d/2)N_p(T_{p,q}\rho)] \cos(p\phi) \end{aligned} \quad (2)$$

The wave fields at the incident side( $z < 0$ ) and the outgoing side ( $z > h$ )of the slab can be expanded as the superposition of all orders of Bloch waves respectively

$$\vec{H}^I = I_{0,0} e^{-i\vec{k}_{||} \cdot \vec{r}_{||}} e^{-ik_{z0,0}z} + \sum_{m=-\infty}^{+\infty} \sum_{n=-\infty}^{+\infty} R_{m,n} e^{-i(\vec{k}_{||} + \vec{G}_{m,n}) \cdot \vec{r}_{||}} e^{-ik_{zm,n}z} \quad (3)$$

$$\vec{H}^{III} = \sum_{m=-\infty}^{+\infty} \sum_{n=-\infty}^{+\infty} T_{m,n} e^{-i(\vec{k}_{||} + \vec{G}_{m,n}) \cdot \vec{r}_{||}} e^{-ik_{zm,n}z} \quad (4)$$

where  $I_{0,0}$  represents the coefficient of incident wave,  $\vec{k}_{||} = k_0 \sin(\theta)\hat{e}_x$  is the in-plane wavevector, while  $k_{z0,0} = \sqrt{k_0^2 - |\vec{k}_{||}|^2}$  is the wavevector along  $z$  axis.  $R_{m,n}$  and  $T_{m,n}$  are the coefficients of the  $(m, n)^{th}$  reflected and transmitted Bloch waves.  $\vec{G}_{m,n} = \hat{e}_x \frac{2\pi m}{p} + \hat{e}_y \frac{2\pi n}{p}$  is the Bloch wavevector of square lattice, where  $\hat{e}_x$  and  $\hat{e}_y$  are the unit vectors of reciprocal space in cartesian coordinate representations. After matching the wave fields of the three regions at two interfaces  $z = 0$  and  $z = h$ , we have

$$\begin{aligned} \sum_{m=-\infty}^{\infty} \sum_{n=-\infty}^{\infty} \Omega_{m,n,p,q} (I_{0,0} \delta_m \delta_n + R_{m,n}) &= a_{p,q} + b_{p,q} \\ \frac{k_{zm,n}}{\varepsilon_0} (I_{0,0} \delta_m \delta_n - R_{m,n}) &= \sum_{p=1}^{\infty} \sum_{q=1}^{\infty} \frac{\Omega_{m,n,p,q}^* \beta_{p,q}}{\varepsilon_r} (a_{p,q} + b_{p,q}) \\ \sum_{m=-\infty}^{\infty} \sum_{n=-\infty}^{\infty} \Omega_{m,n,p,q} T_{m,n} &= a_{p,q} e^{-i\beta_{p,q}h} + b_{p,q} e^{i\beta_{p,q}h} \\ \frac{k_{zm,n}}{\varepsilon_0} T_{m,n} &= \sum_{p=1}^{\infty} \sum_{q=1}^{\infty} \frac{\Omega_{m,n,p,q}^* \beta_{p,q}}{\varepsilon_r} [a_{p,q} e^{-i\beta_{p,q}h} - b_{p,q} e^{i\beta_{p,q}h}] \end{aligned} \quad (5)$$

where  $\Omega_{m,n,p,q} = \int_0^{2\pi} d\phi \int_a^b d\rho e^{i(\vec{k}_{\parallel} + \vec{G}_{m,n}) \cdot \vec{r}_{\parallel}} \vec{g}_i^*(\rho, \phi)$  is an overlap integral, denoting the coupling coefficient from a Bloch wave channel  $(m, n)^{th}$  to a guided wave channel  $(p, q)^{th}$ . We expand a plane wave  $e^{-ik_{\parallel}\rho \cos(\phi-\theta)}$  in the form of  $\sum_{l=0}^{\infty} \frac{1}{l!} [-ik_{\parallel}\rho \cos(\phi-\theta)]^l$  in cylinder coordinates to solve EQs(5). Then we derived coefficients of the transmitted or reflected Bloch waves for the linear EQs(5)

$$\begin{aligned} T_{m,n} &= \Omega_{m,n,p,q}^* \frac{k_{z_{m,n}}}{\beta_{p,q}} (a_{p,q} e^{-i\beta_{p,q}h} - b_{p,q} e^{i\beta_{p,q}h}) \\ R_{m,n} &= I_{0,0} \delta_m \delta_n - \Omega_{m,n,p,q} \frac{k_{z_{m,n}}}{\beta_{p,q}} (a_{p,q} - b_{p,q}) \end{aligned} \quad (6)$$

As surface resonances are intrinsic properties of the system, we can extract the dispersion of surface resonances by assigning a zero value to the incidence, i.e., omitting the term  $I_{0,0} e^{i\vec{k}_{\parallel} \cdot \vec{r}_{\parallel}} e^{-ik_{z_{0,0}}z}$  in EQ(3), and solving the eigen-value of EQs(5).

#### IV. EVEN-MODE OR ODD-MODE SURFACE RESONANCES

Circular dots and solid lines in Fig.1) presented the measured and calculated transmission spectra under normal incidence ( $\theta = 0^\circ$ ) for samples with different inner diameters  $d = 8.3, 6.3, 5.0, 2.0$ mm. For the sample with  $d = 8.3$ mm, the measured transmission peak reaches unity at 8.64GHz (*Fig.1a*). When the inner diameter  $d$  becomes smaller, the transmission peak at 8.64GHz becomes blue-shifted. In good agreement with the peak and lineshape of the measured curves, the calculated transmission spectra also possess two narrow transmission peaks with fano lineshape at 9.99GHz and 14.12GHz irrespective to the inner diameter  $d$ . These additional transmission peaks are scaled by periodicity of the structure. Fig.2) presents frequencies of the transmission peaks under normal incidence ( $\theta = 0^\circ$ ) with respect to different inner diameters  $d$ . We calculate the spatial field distributions on the slab to better understand the formation and the underlying mechanism of these two kinds of transmission peaks. *Fig3*) presents the electric field component and the power flow component in  $xz$  plane on the slab surface with respect to the two transmission peak at 8.64GHz and at 9.99GHz. For the narrow resonant peak at 9.99GHz, calculations on the spatial field distribution show that the electric field component along  $z$  axis is anti-symmetric to the  $z = \frac{h}{2}$  plane at both sides of the plate, which is rightly the field distribution of an odd-mode surface resonance [15], as shown in *Fig.3b*) and *Fig.3d*). It is reasonable that its frequency is mainly decided by the periodicity and symmetry of the array, and indifferent to the local geometry of apertures, in that most field energy near the metallic surface distributes far from the apertures with the minimum in them, as shown in Fig.3d). In other words, the odd-mode surface resonance is almost blind to the aperture. While the shifted broad transmission peaks in *Fig.2*) come from the even-mode surface resonant states in that the electric field component along  $z$  axis is symmetric to the  $z = \frac{h}{2}$  plane at both sides of the plate with most field energy localized inside the aperture as well as its vicinity near the surface, as shown in *Fig.3a*) and *Fig.3c*) for the transmission peak at 8.64GHz respectively. The normalized strength of the radial gap width  $(D-d)/2$ . The field enhancement may be applied to the near-field probing or nonlinear optics [16]. The frequency of an odd-mode surface resonance  $f_{m,n}^{Odd}(k_x)$  is slightly lower than Rayleigh frequency  $f_{m,n}^{Rayleigh}(k'_{//}) = \frac{c}{p} \sqrt{(k'_x + m)^2 + (k'_y + n)^2}$  where Wood anomaly happens [17, 18],  $k'_{//} = (k_x, k_y) \cdot p / (2\pi)$  is the normalized wavevector. For example, at  $k_x = k_y = 0$ ,  $f_{1,0}^{Rayleigh} \simeq 9.993$ GHz is slightly higher than  $f_{1,0}^{Odd} \simeq 9.990$ GHz for the array of holes ( $d = 8.3$ mm). With the increase of  $d$ , the frequency  $f_{m,n}^{Odd}(k'_{//})$  suffers an imperceptible blue-shift. All the even-mode branches in *Fig.2*) are confined within the intervals divided by the frequencies  $\{f_{m,n}^{Odd}\}$  of odd-mode surface resonances, and tends to asymptotic to the lower bound with the increase of  $d$ . The features imply that the even-mode surface resonances are the collective selections on the interplay between the waveguide resonance and in-plane evanescent diffractive channels.

#### V. ANGULAR DEPENDENT TRANSMISSION SPECTRA AND DISPERSION DIAGRAM OF SURFACE RESONANCES

We calculate the dispersion diagram of surface resonances for all polarizations, as shown in the solid or dashed lines in Fig.4) for the even-mode or odd-mode surface resonant states. We also measured the transmission spectra through all four samples under oblique incidence. The measured transmissivity is plotted in colormap as a function of frequency and the in-plane wavevector  $\vec{k}_{\parallel} = \frac{2\pi f}{c_0} \sin(\theta) \hat{e}_x$ , converted from the incident angle  $\theta$ . For the sample of

$d = 8.3\text{mm}$ , a transmission peak at  $f = 8.64\text{GHz}$  in  $TE$  polarization is not shifted almost under any incidence angles (see *Fig.4a*), reaching unity at normal incidence with  $\theta = 0^\circ$ . A similar result has been predicted in a previous study on the rectangular holes[10]. For the other three samples, the first transmission peak in  $TE$  polarization becomes dispersive alternatively with respect to the incident angles, the experimental data for  $d = 6.3, 5.0, 2.0\text{mm}$  is shown in *Fig.4c, 4e, 4g*) respectively. It implies that the local resonance of the sample with  $d = 8.3\text{mm}$  lies below the limit of Rayleigh frequency while above it for other samples, as we know that a local resonance will couple with different Bloch channels when it is below or above Rayleigh frequency.

Below the limit of Rayleigh frequency  $f_{1,0}^{\text{Rayleigh}}$ , there only exist  $\vec{G}(-1, 0)$  and  $\vec{G}(0, 0)$  Bloch channels. Without the projection of wave vector component of the incidence along  $y$  axis, the  $TE$  polarized waves incident in the  $y = 0$  plane can not couple with these Bloch channels. So for  $d = 8.3\text{mm}$ , without the assistance from any Bloch channels, we can observe a flat polariton branch in  $TE$  mode, as shown in *Fig.4a*). Meanwhile the  $TM$  polarized incidence in the  $y = 0$  plane can be coupled to the  $\vec{G}(-1, 0)$  Bloch channel due to the same reason; the  $TM$  polarized surface resonant states in even mode comes from the interference between the waveguide resonance and the  $\vec{G}(-1, 0)$  Bloch channels, giving rise to two anti-symmetric asymptotic branches in *Fig.4b*). The bright curvatures for measured data prove the existence of the two branches, as shown *Fig.4b*). Thus the role of local resonance on the surface waves below  $f_{1,0}^{\text{Rayleigh}}$  is revealed.

More diffractive channels lie above  $f_{1,0}^{\text{Rayleigh}}$ , such as  $\vec{G}(0, \pm 1)$ , and  $\vec{G}(\pm 1, \pm 1)$  etc. When  $d$  becomes smaller, the waveguide resonance will shift across  $f_{1,0}^{\text{Rayleigh}}$  from below.  $TE$  polarized incidence will couple with the waveguide resonance via  $\vec{G}(0, \pm 1)$ , and  $\vec{G}(-1, \pm 1)$  channels, resulting in different features of dispersion diagrams and transmission spectra. As an example, for the sample with  $d = 6.3\text{mm}$ , the three branches below  $f_{1,1}^{O_{dd}} = 14.12\text{GHz}$  are rightly the consequence of the interplay between the local resonance and the  $\vec{G}(0, \pm 1)$ ,  $\vec{G}(-1, \pm 1)$  channels under  $TE$  polarized incidence. As shown in *Fig.4c*), the bright-colored curvature exactly fits the curve of the lowest branch with the brightest point at the location ( $k_x = \pi/p$ ,  $f = 9.97\text{GHz}$ ), which is the four-fold degenerate point about  $\vec{G}(-1, \pm 1)$ , and  $\vec{G}(0, \pm 1)$ . The maximal transmissivity at the Brillouin zone boundary means that the strongest coupling between the local resonance and the Bloch channels is likely to occur at the degenerate states with high symmetry. The coupling between local resonance and diffractive channels will induce highly inhomogeneous field distribution on the surface, resulting in the opening of bandgaps, similar to the case of corrugated metallic surface [19]. As shown in *Fig.4c*), existence of two bandgaps between the three branches verifies the analysis. The coupling will inevitably induce the split of the frequency at the degenerate points. We notice that right above the ‘‘brightest’’ state ( $k_x = \pi/p$ ,  $f = 9.97\text{GHz}$ ), the second  $TE$  polarized branch in even mode converges with four odd-mode branches ( $-1, \pm 1$ ) and  $(0, \pm 1)$  at the degenerate state ( $k_x = \pi/p$ ,  $f = 11.12\text{GHz}$ ) on BZ boundary. The degeneracy demonstrates that the state also possesses anti-symmetric distribution of the spatial field and minimum transmissivity. It also applies for *Fig.4e*) and *Fig.4g*); the superposed bright curvature on the second branch becomes weaker, reaching minimum at the four-fold degenerate state. The rule governs all dispersion diagrams in  $TM$  polarization, on the second branch at  $k_x = \pi/p$ , the third branch at  $k_x = \pi/2p$  and  $k_x = 3\pi/2p$ , the fourth branch at  $k_x = \pi/2p$  in *Fig.4b,d,f,h*). Transmission extrema at the degenerate states are understandable. Considering these brightest states with four-fold degeneracy, they are likely to couple with the incident waves with strongly localized field within the apertures and have zero group velocity along any direction within the  $xy$  plane. Meanwhile, the odd-mode surface resonant states are invisible in measurements, and the geometry of apertures has little impact on the odd-mode branches.

## VI. CONCLUSION

In summary, we perform microwave experiments and rigorous modal expansion method to investigate the enhanced microwave transmission through the array of metallic coaxial annular apertures (MCAAs) as well as the dispersion of surface resonances. The even-mode and the odd-mode surface resonances are clarified theoretically by the spatial field distributions and the dispersion diagram. The impact of local resonance is thoroughly embodied in the even-mode surface resonant states. While the odd-mode surface resonant states, invisible in measurements, are scaled by periodicity, invariant to different local geometry of the unit cell. The enhanced transmission is the collective selections on the interplay between the local resonances and the evanescent Bloch channels on the surface. Transmissivity reaches extrema at the degenerate points in the dispersion diagram of surface resonances. The work provides a holistic description on the interplay between the local resonance and the plane wave excitations via evanescent Bloch channels.

### Acknowledgments

This work was supported by the National 863 Program of China (Grant No.2006AA03Z407), NSFC (Grant No.10574099, No.60674778), CNKBRF(Grant No.2006CB921701), NECT, STCSM and Shanghai Education and Development Foundation (No. 06SG24).

- 
- [1] T. W. Ebbesen, H. J. Lezec, H. F. Ghaemi et al., "Extraordinary optical transmission through sub-wavelength hole arrays," *Nature* 391,667-669 (1998).
  - [2] H. F. Ghaemi, T. Thio, D. E. Grupp et al., "Surface plasmons enhance optical transmission through subwavelength holes," *Phys. Rev. B* 58,6779-6782 (1998).
  - [3] J. A. Porto, F. J. Garcia-Vidal, and J. B. Pendry," Transmission Resonances on Metallic Gratings with Very Narrow Slits," *Phys. Rev. Lett.* 83,2845 (1999).
  - [4] M. Beruete, M. Sorolla, I. Campillo et al., "Enhanced millimeter wave transmission through quasioptical subwavelength perforated plates," *IEEE Trans. Antennas Propag.* 53,1897-1903 (2005).
  - [5] J. B. Pendry, L. Martin-Moreno, and F. J. Garcia-Vidal," Mimicking surface plasmons with structured surfaces," *Science* 305,847-848 (2004).
  - [6] F. I. Baida, D. Van Labeke, G. Granet et al., "Origin of the super-enhanced light transmission through a 2-D metallic annular aperture array: a study of photonic bands," *Appl. Phys. B* 79,1-8 (2004).
  - [7] W. J. Fan, S. Zhang, B. Minhas et al., "Enhanced infrared transmission through subwavelength coaxial metallic arrays," *Phys. Rev. Lett.* 94,033902 (2005).
  - [8] K. J. K. Koerkamp, S. Enoch, F. B. Segerink et al., "Strong influence of hole shape on extraordinary transmission through periodic arrays of subwavelength holes," *Phys. Rev. Lett.* 92,183901 (2004).
  - [9] K. L. van der Molen, K. J. Klein Koerkamp, S. Enoch et al., "Role of shape and localized resonances in extraordinary transmission through periodic arrays of subwavelength holes: Experiment and theory," *Phys. Rev. B* 72,045421 (2005).
  - [10] Z. C. Ruan and M. Qiu," Enhanced transmission through periodic arrays of subwavelength holes: The role of localized waveguide resonances," *Phys. Rev. Lett.* 96,233901 (2006).
  - [11] R. Gordon, A. G. Brolo, A. McKinnon et al., "Strong polarization in the optical transmission through elliptical nanohole arrays," *Phys. Rev. Lett.* 92,037401 (2004).
  - [12] P. Sheng, R. S. Stepleman, and P. N. Sanda, "Exact eigenfunctions for square-wave gratings: Application to diffraction and surface-plasmon calculations," *Physical Review B* 26, 2907 (1982).
  - [13] P. Lalanne, J. P. Hugonin, S. Astilean, M. Palamaru, and K. D. Moller, "One-mode model and Airy-like formulae for one-dimensional metallic gratings," *J Opt a-Pure Appl Op* 2, 48-51 (2000).
  - [14] J. D. Jackson, *Classical Electrodynamics* (John Wiley & Sons, New York, 1999).
  - [15] L. Martin-Moreno, F. J. Garcia-Vidal, H. J. Lezec et al., "Theory of Extraordinary Optical Transmission through Sub-wavelength Hole Arrays," *Phys. Rev. Lett.* 86, 1114-1117 (2001).
  - [16] J. A. H. van Nieuwstadt, M. Sandtke, R. H. Harmsen et al., "Strong modification of the nonlinear optical response of metallic subwavelength hole arrays," *Phys. Rev. Lett.* 97, 146102 (2006).
  - [17] R W Wood," On a Remarkable Case of Uneven Distribution of Light in a Diffraction Grating Spectrum," *Proceedings of the Physical Society of London* 269 (1902).
  - [18] R. W. Wood," Anomalous Diffraction Gratings," *Physical Review* 48,928-936 (1935).
  - [19] W. L. Barnes, T. W. Preist, S. C. Kitson et al., "Physical origin of photonic energy gaps in the propagation of surface plasmons on gratings," *Phys. Rev. B* 54, 6227-6244 (1996).

## Figure captions:

FIG.1. Simulated (lines) and Measured (open circles) transmission spectra through the array of MCAAs with different inner diameter  $d = 8.3\text{mm}$ (a),  $6.3\text{mm}$ (b),  $5.0\text{mm}$ (c),  $2.0\text{mm}$ (d) respectively. The inset presents the photo of the sample ( $d = 8.3\text{mm}$ )

FIG.2. Resonant frequencies of even mode (solid lines) and odd mode (dashed lines) under normal incidence ( $k_{\parallel} = 0$ ) with respect to the inner diameter  $d$  varying in the range of  $0.0 \sim 4.9\text{mm}$ . The measured frequencies for different samples are marked with stars.

FIG.3. Spatial field distributions of the even/odd surface mode in  $xz$  plane for the sample with  $d = 8.3\text{mm}$ . (a) E field, even; (b) E field, odd; (c) Power flow, even; (d) Power flow, odd

FIG.4. Dispersion relations of even surface resonances (solid lines) and odd surface surface resonances (dashed lines) for samples with different inner diameter  $d = 8.3, 6.3, 5.0, \text{ and } 2.0\text{mm}$ . (a), (c), (e), (g) for  $TE$  polarization and (b), (d), (f), (h) for  $TM$  polarization. Frequency  $f$  is normalized to the limit of Rayleigh frequency  $c_0/p = 9.993\text{GHz}$ . Measured transmittivities with respect to the in-plane wave vector and frequency are plotted in color-scale.

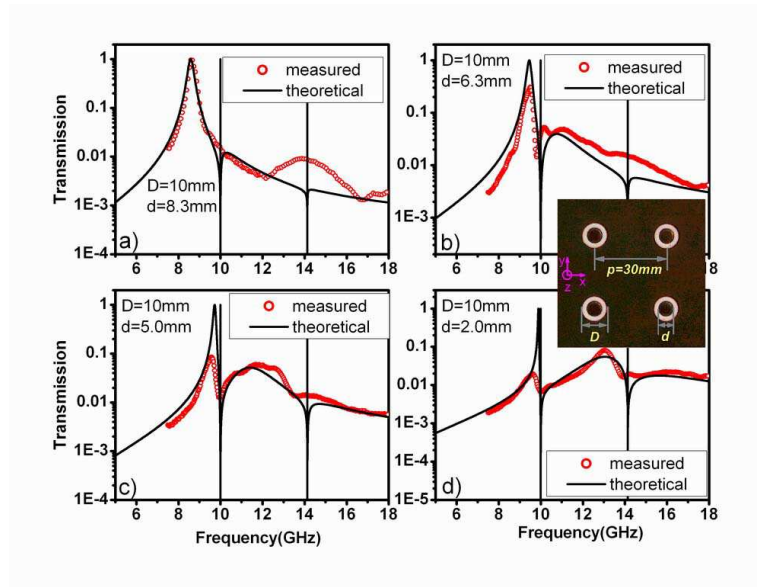


FIG.1. Simulated (lines) and Measured (open circles) transmission spectra through the array of MCAAs with different inner diameter  $d = 8.3\text{mm}$ (a),  $6.3\text{mm}$ (b),  $5.0\text{mm}$ (c),  $2.0\text{mm}$ (d) respectively. The inset presents the photo of the sample ( $d = 8.3\text{mm}$ )

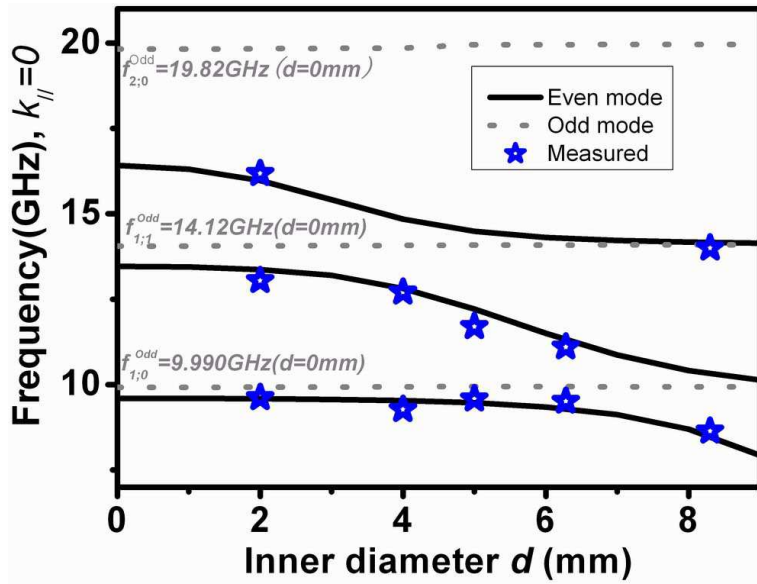


FIG.2. Resonant frequencies of even mode (solid lines) and odd mode (dashed lines) under normal incidence ( $k_{\parallel} = 0$ ) with respect to the inner diameter  $d$  varying in the range of  $0.0 \sim 4.9\text{mm}$ . The measured frequencies for different samples are marked with stars.

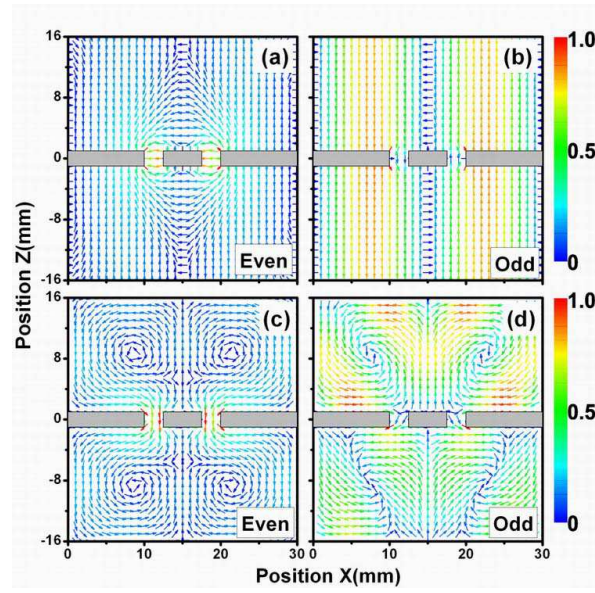


FIG.3. Spatial field distributions of the even/odd surface mode in  $xz$  plane for the sample with  $d = 8.3\text{mm}$ . (a) E field, even; (b) E field, odd; (c) Power flow, even; (d) Power flow, odd

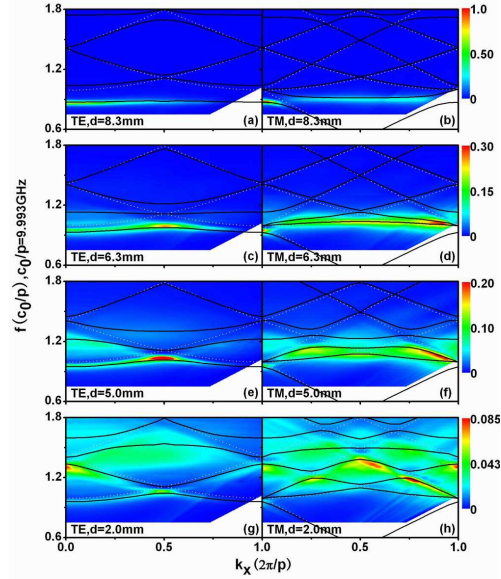


FIG.4. Dispersion relations of even surface resonances (solid lines) and odd surface resonances (dashed lines) for samples with different inner diameter  $d = 8.3, 6.3, 5.0,$  and  $2.0\text{mm}$ . (a), (c), (e), (g) for  $TE$  polarization and (b), (d), (f), (h) for  $TM$  polarization. Frequency  $f$  is normalized to the limit of Rayleigh frequency  $c_0/p = 9.993\text{GHz}$ .

Measured transmittivities with respect to the in-plane wave vector and frequency are plotted in color-scale.